ACS APPLIED MATERIALS & INTERFACES

Research Article

www.acsami.org

Vesicular Self-Assembly of Colloidal Amphiphiles in Microfluidics

Jie He,[†,∥] Lei Wang,[†,‡,∥] Zengjiang Wei,[†,§] Yunlong Yang,[†] Chaoyang Wang,[§] Xiaojun Han,[‡] and Zhihong Nie*[,†]

[†]Department of Chemistry and Biochemistry, University of Maryland, College Park, Maryland 20742, United States

[‡]School of Chemical Engineering and Technology, Harbin Institute of Technology, Harbin 150001, China

[§]Research Institute of Materials Science, South China University of Technology, Guangzhou 510640, China

Supporting Information

ABSTRACT: Hydrodynamic flow in a microfluidic (MF) device offers a high-throughput platform for the continuous and controllable self-assembly of amphiphiles. However, the role of hydrodynamics on the assembly of colloidal amphiphiles (CAMs) is still not well understood. This Article reports a systematic study of the assembly of CAMs, which consist of Au nanoparticles (AuNPs) grafted with amphiphilic block copolymers, into vesicles with a monolayer of CAMs in the membranes using laminar flows in MF flow-focusing devices. Our experimental and simulation studies indicate that the transverse diffusion of solvents and colloids across the boundary of neighboring lamellar flows plays a critical role in the assembly of CAMs into vesicles. The dimension of the vesicles can be controlled in the range of 100−600 nm by tuning the hydrodynamic conditions of the flows. In addition, the diffusion coefficient of CAMs was also critical for their assembly. Under the same flow conditions, larger CAMs generated larger assemblies as a result of the reduced diffusion rate of large amphiphiles. This work could provide fundamental guidance for the preparation of nanoparticle vesicles with applications in bioimaging, drug delivery, and nano- and microreactors.

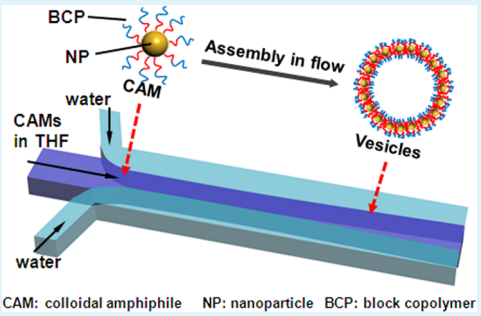

KEYWORDS: *microfluidics, hydrodynamic flow, colloidal amphiphiles, amphiphilic nanoparticles, self-assembly, vesicles*

INTRODUCTION

Colloidal amphiphiles (CAMs) composed of inorganic nanoparticle (NP) cores and amphiphilic polymer or block copolymer (BCP) tethers, represent a new class of building blocks for assembling functional materials.[1−11] The self-assembly of CAMs resembles but differs from that of conventional linear molecular amphiphiles (e.g., lipids and amphiphilic BCPs) because of their unique geometry and significantly increased dimension and rigidity.[2] CAMs can assemble into nanostructures with various morphologies such as clusters, vesicles, and tubules in a selective solvent.[1−8] The organization of CAMs offers a new paradigm for controlling the collective optoelectronic properties of NP ensembles.[12−19] For instance, the assembly of CAMs containing gold NPs (AuNPs) leads to the shift or splitting of the localized surface plasmon resonance (LSPR) band of the assembled structures because of the strong plasmon coupling between adjacent NPs.[8,20] The fine tuning of the LSPR enables the application of such NP ensembles in areas including surface-enhanced Raman scattering,[21] bioimaging, and photothermal therapy for cancer treatment.[22−25] However, current bottom-up strategies (including solvent mixing, dialysis, and film rehydration)[1,4,26,27] for the assembly of CAMs typically show limited control over the size, morphology, and property of the assemblies.

Microfluidics (MFs) has been applied for the continuous assembly of molecular amphiphiles.[27−34] The unprecedented control over the sizes and morphologies of assemblies is attributed to the precise manipulation of the fluid mixing using laminar flows.[27] Recently, our group demonstrated the continuous assembly of CAMs consisting of Au nanorods (AuNRs) tethered with BCPs in MFs.[35] The fluid mixing plays a critical role in controlling the assembly pathways of CAMs because of the slow diffusion of the relatively large-sized CAMs. This approach enables control over the kinetic pathways of CAM assembly to generate assemblies with various morphologies, including spherical micelles, giant vesicles, and raftlike disks, by adjusting the hydrodynamic conditions.[35] In addition, MFs offers a way to explore the intermediated states of assembly by quenching the assemblies of CAMs at various stages of assembly. Nevertheless, it is still unclear what determines the final structures of the MF self-assembly of CAMs.

This Article describes a systematic investigation of the self-assembly of CAMs composed of spherical AuNPs tethered with amphiphilic BCPs using MF flow-focusing devices (MFFDs). The CAMs assembled into vesicular structures with a monolayer of AuNPs in the membranes under a wide range of hydrodynamic conditions. Our experiments and simulations demonstrated that both the flow rates of the fluids and the size-dependent diffusion rate of the CAMs have a significant impact

Received: July 18, 2013
Accepted: September 9, 2013
Published: September 9, 2013

   dx.doi.org/10.1021/am4028839 | ACS Appl. Mater. Interfaces 2013, 5, 9746−9751

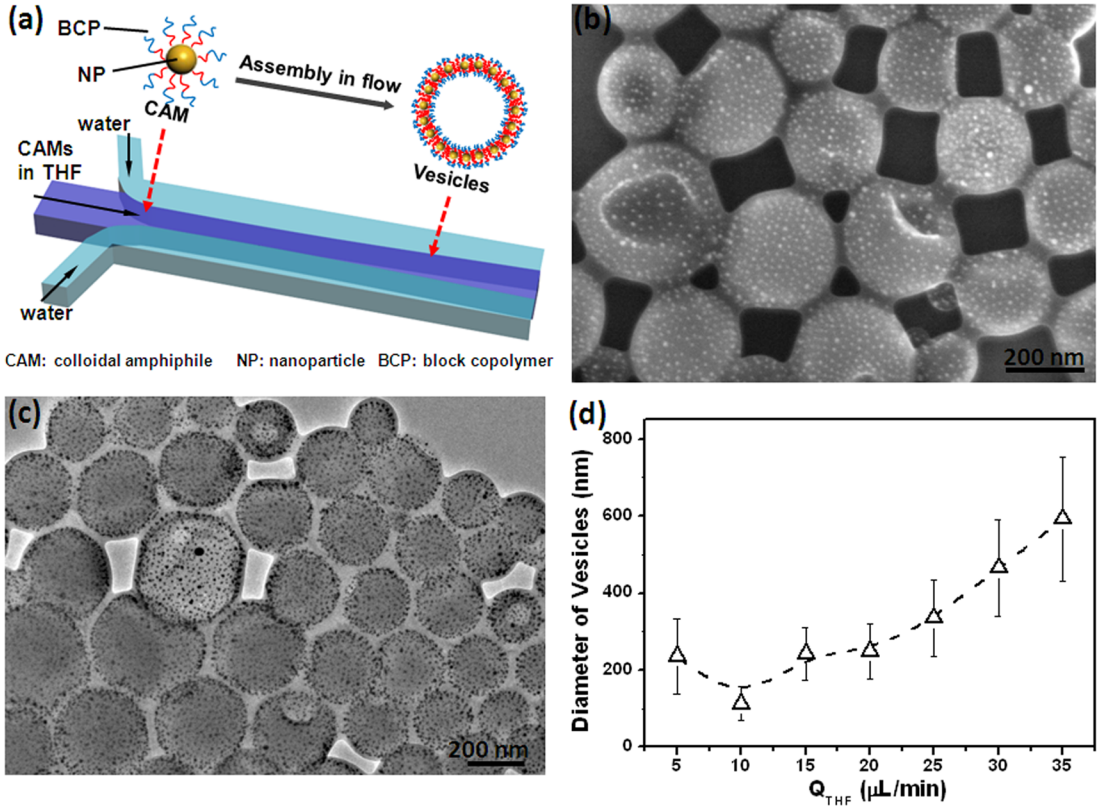

Figure 1. (a) Schematic illustration of the self-assembly of CAMs into vesicular assemblies in MFFDs. The CAMs of AuNPs tethered with BCPs were dispersed in THF. (b, c) Representative SEM (b) and TEM (c) images of vesicles assembled from CAMs containing 5 nm AuNPs modified with PEO_{45}-b-PS_{455}-SH at Q_{THF} = 15 μL/min and Q_{H_2O} = 45 μL/min. (d) Size of the vesicles as a function of Q_{THF} at a constant Q_{H_2O} of 45 μL/min. The size of the vesicles at each point was averaged from more than 100 vesicles.

on the assembly of CAMs in MFFDs. The size of the vesicular assemblies of CAMs can be controlled in the range of 100−600 nm by varying the flow rates of fluids and the diffusion coefficient of CAMs. At a low flow rate of the center flow containing CAMs, the strong focusing effect rapidly depleted the center flow, resulting in the formation of smaller assemblies. In contrast, at a high flow rate of the center flow, the slow diffusive mixing between neighboring streams led to the formation of large assemblies. In addition, we found that the size-dependent diffusion coefficient of CAMs strongly influenced their diffusive mixing between neighboring flows. A smaller diffusion coefficient for the larger CAMs led to the formation of larger vesicular assemblies as a result of the slower depletion of CAMs.

EXPERIMENTAL SECTION

Design of Microfluidic Devices. MFFDs were fabricated using a standard soft-lithography method.[36] The master with relief patterns was fabricated with SU-8 resin on a silicon wafer using photolithography. Poly(dimethylsiloxane) (PDMS)-based MF devices were then replicated from the master. In brief, a 10:1 (weight ratio) mixture of silicone elastomer oligomer and crosslinker (Sylgard 184 Silicone Elastomer Kit, Dow Corning) was poured onto the master and cured at 65 °C overnight. The PDMS replica was then peeled off from the master and bonded onto a glass or PDMS substrate and was immediately after treated by oxygen plasma for 2 min. The dimensions of the microfluidic devices are as follows (see Scheme S1). The distances from the inlets to the junctions were 1.7 and 10 mm for the main channels and the side channels, respectively. The length of the main channel was 346.5 mm in total. The height of channels and the width of main channel and side channels were 100, 330, and 120 μm, respectively.

Preparation and Self-Assembly of CAMs. Five nanometer AuNPs were synthesized via seed-mediated growth using a reported procedure.[37] CAMs were prepared by modifying AuNPs with BCPs of poly(ethylene oxide)-b-poly(styrene) terminated with thiol groups (PEO_{45}-b-PS_{455}-SH) using an interfacial ligand-exchange method.[4,10] Typically, 5 mg of BCPs was first dissolved in 10 mL of chloroform, which is immiscible with water. This solution was added into an aqueous solution of AuNPs followed by sonication for 2 h to form emulsions at room temperature. The solution of emulsions was kept undisturbed overnight. The organic and water phases spontaneously separated into two layers, and the water phase became colorless. The organic phase containing AuNPs modified with BCPs was then collected and dried under vacuum at 40 °C. The BCP-modified AuNPs were dispersed in tetrahydrofuran (THF) and further purified by centrifugation in THF/water/ethanol (2:1:2, vol %) for six cycles.

The self-assembly of CAMs was performed in PDMS-based MFFDs. Water was introduced from two side channels, and a THF solution of CAMs (ca. 0.5 mg/mL) was injected from a central channel into the device using syringe pumps. The samples of the assembled structures were collected from the outlet channel of the MFFDs after the flow of fluids became stable upon varying the flow rates of the fluids. The samples were then imaged using a Hitachi SU-70 Schottky field-emission gun (FEG) Scanning Electron Microscope (SEM) and a JEOL FEG Transmission Electron Microscope (TEM). Samples for SEM imaging were prepared by casting a 5−10 μL of sample solution on silicon wafers and were dried at room temperature. TEM samples were prepared by casting on 300 mesh copper grids covered with carbon film and were dried at room temperature.

Simulations. COMSOL Multiphysics 4.3 (COMSOL, Inc., Burlington, MA) was used to simulate the microfluidic mixing between the miscible water stream and the CAM-containing THF

stream in a 2D model. The simulations were conducted following the method reported previously.[27] A two-phase fluid-flow system was simplified as a single-phase system with concentration-dependent diffusion or viscosity. The CAMs were approximated as uniformly spherical in shape, and their diameters were calculated by summing the size of the AuNP cores and the thickness of the polymer shells.

The concentration distribution of fluids was modeled in the convection and diffusion modes using the steady-state incompressible Navier–Stokes equation.[27,38] A single-phase model was adopted for all of the simulations with continuous shear force and velocity across the contact interface and the microchannel, which is described by the following equations

$$-\nabla\eta(\nabla\mathbf{u} + (\nabla\mathbf{u})^T) + \rho(\mathbf{u}\nabla)\mathbf{u} + \nabla p = 0 \quad (1)$$

$$\nabla\mathbf{u} = 0 \quad (2)$$

$$-\nabla(-D\nabla c + c\mathbf{u}) = 0 \quad (3)$$

where η represents the dynamic viscosity, $\mathbf{u}$ denotes the velocity vector, ρ is the density, p is the pressure, and D and c are the mutual diffusivity and the concentration of fluids, respectively. The simulation condition was set as no-slip and no-penetration boundary as well as zero diffusional flux at the wall of the channel. Another two assumptions utilized in our simulations are (i) a homogeneous mixing of THF and water on the microscale, regardless the micro-heterogeneities on the molecular scale and (ii) a constant single-phase density, neglecting any possible diffusion-induced convection.[27]

The parameters in the simulations were set as follows. The size of the microfluidic device is the same as that used in the experiments. The flow rates of fluids in the main channel and the side channels were predetermined, as described in Experimental Section. The meshing course was completed with a maximum element size of 16 μm, a minimum element size of 0.8 μm, a maximum element growth rate of 1.05, a resolution of curvature of 0.2, and a resolution of 1.0 in the narrow regions. The diameter of CAMs is 61 nm, including 5 nm of the Au cores and 28 nm of the polymer shell. The diffusion coefficient, D, of spherical particles through liquid with a low Reynolds number was calculated using the Stokes–Einstein equation

$$D = \frac{kT}{6\pi\eta r} \quad (4)$$

where k is the Boltzmann constant, T is the absolute temperature, and η and r are the viscosity and radius of the spherical particle, respectively.

RESULTS AND DISCUSSION

The CAMs used in this study are composed of AuNPs (5 or 20 nm in diameter) tethered with linear amphiphilic BCPs of PEO_{45}-b-PS_{455} (Mn = 49.3 kg/mol and PDI = 1.18) with a thiol group at the PS end. The CAMs were prepared by tethering BCPs onto the surface of AuNPs using the ligand-exchange method and were dispersed in THF. The assembly of CAMs was triggered by focusing a THF solution of CAMs (ca. 0.5 mg/mL) between two streams of water (nonsolvent for PS blocks) to enter a common outlet channel in the MFFDs (Figure 1a). Two fluids formed a laminar flow because of the low Reynolds number in the microchannels.[39] The diffusive mixing between two miscible liquids along the transverse direction changed the quality of the solvents for PS blocks of BCP tethers at the biphasic boundary, leading to the simultaneous self-assembly of CAMs.

The CAMs continuously assembled into vesicles over a wide range of flow rates in MFFDs. The self-assembly of CAMs was driven by the spontaneous anisotropy and directional interactions between CAMs resulting from the stretching and packing of the flexible polymer chains on the surface of AuNPs. SEM and TEM images in Figure 1b,c show the representative vesicular assemblies of CAMs with 5 nm AuNP core at Q_{H_2O} = 45 μL/min and Q_{THF} = 15 μL/min. The vesicles are composed of a single layer of AuNPs in the membranes. The average diameter of vesicles is 241.7 ± 68.4 nm. The hollow interior of the assemblies is apparently similar to that of polymer vesicles. During drying, the membrane of the vesicles flattened and formed pancakelike structures on the substrate.[7] Both the size of the vesicles and interparticle distance of the adjacent AuNPs in the membranes of vesicles obtained by this approach are clearly larger than those of vesicular assemblies prepared by the film-rehydration or solvent-mixing methods reported previously.[4,8,40] We presume that this is due to the swelling of PS blocks in the presence of THF. The vesicular assemblies are quite stable in the mixed solvents, and the structural integrity is not changed at all after they are stored for 3 months.

Unlike the direct mixing of solvents in a conventional assembly, the MF approach enables the precise control over the diffusive mixing of solvents and colloids at the interface of two laminar flows by tuning the hydrodynamic conditions. The transverse diffusion of two streams can be quantitatively described by the mixing time (t_{mix}). In the region of hydrodynamic focusing, t_{mix} can be estimated by[32]

$$t_{mix} \sim \frac{w_f}{4D} \approx \frac{w^2}{9D(1 + 1/R)^2} \quad (5)$$

where w_f, w, D, and R are the width of the central stream, the width of the downstream channel, the diffusion coefficient of water–THF, and the flow-rate ratio of the THF-to-water stream ($R = Q_{THF}/Q_{H_2O}$), respectively. A large value of t_{mix} represents a slow mixing of the solvents and colloids between two neighboring flows through the transverse diffusion. The kinetics of the assembly of CAMs in MFFDs is largely determined by how fast the CAMs will diffuse to interact with water.[27,32] When t_{mix} is small, CAMs can quickly interact with water, resulting in a fast quenching of self-assembly to form smaller structures. When t_{mix} is large, a long mixing time allows the continuous recruitment of CAMs to form larger assemblies. In other words, the parameters (e.g., Q_{THF}, Q_{H_2O}, and the diffusion coefficient of solvent/CAMs) that affect the diffusion of the fluids and colloids have great impacts on the MF self-assembly of CAMs.

To understand the influence of the hydrodynamic conditions on the assembly morphologies, we studied the effect of Q_{THF} and Q_{H_2O} on the self-assembly of CAMs. First, at a Q_{H_2O} of 45 μL/min and 5 ≤ Q_{THF} ≤ 20 μL/min, the diameter of the vesicles was weakly dependent on Q_{THF}, as shown in Figure 1d (see Figures S1–S4 for the SEM and TEM images). For Q_{THF} ≥ 20 μL/min, the size of the vesicles increased significantly from 248.8 ± 71.5 to 592.3 ± 161.8 nm with the increase of Q_{THF} (Figure S6). It is also noted that the variation in vesicle size was accompanied with an increase in the polydispersity of the vesicles. A similar trend was also observed for assembly at a Q_{H_2O} of 90 μL/min (Figure S7). The size of the assemblies was almost independent on Q_{THF} at 20 ≤ Q_{THF} ≤ 50 μL/min, whereas the size significantly increased with the increase of Q_{THF} at Q_{THF} ≥ 50 μL/min. The diameter of the vesicles increased from 113.6 to 271.2 nm with the increase of Q_{THF} from 50 to 90 μL/min. However, the size of the vesicles prepared at a Q_{H_2O} of 90 μL/min was much smaller than that of vesicles obtained at a Q_{H_2O} of 45 μL/min even at the same flow-

rate ratio of the water-to-THF phase. We ascribed this to the enhanced mixing of two streams at a higher Péclet number ($Pe \propto Q_{total} = Q_{H_2O} + Q_{THF}$) resulting from the increase in the total flow rate of the two streams.[41]

The microfluidic mixing of two miscible streams in MFFDs was simulated using COMSOL Multiphysics 4.3 to gain more insight into the kinetics of mixing and their effects on the assembly kinetics of CAMs. We approximated that the diffusion of two neighboring streams occurred only within the 2D plane in the transverse direction as an ideal laminar flow. Figure 2a shows the concentration distribution of CAMs at various Q_{THF} and a constant Q_{H_2O} of 45 μL/min. At a low Q_{THF} (<20 μL/min), the strong focusing imposed on the central flow by the two side water streams resulted in a narrow THF stream and a short focusing length (top two in Figure 2a). The rapid depletion of the THF stream led to a short t_{mix} of two streams and a rapid assembly of CAMs within the flow focusing length. In this case, most CAMs assembled in the flow-focusing region to generate smaller vesicles because of the rapid quenching of the assembly process with a large amount of water. The increase of Q_{THF} decreased the focusing effect and widened the THF stream (Figure 2a). In this case, the concentration of CAMs (as well as THF) remained high in the center of the THF stream. Only a small fraction of CAMs assembled in the flow-focusing region to form small vesicles, whereas the majority of CAMs assembled into large vesicles in the downstream region where the mixing between neighboring phases is dominated by the diffusion. Figure 2b displays the concentration profiles of CAMs as a function of the transverse coordinates at various flow rates of the THF stream. The concentration of CAMs in the central flow dramatically decreased with reducing Q_{THF}.

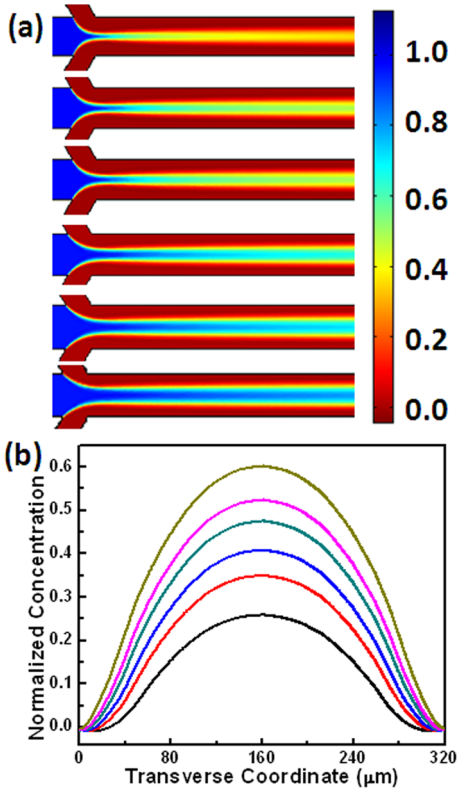

Figure 2. Simulated CAM concentration distribution at various flow rate ratios of the water to THF phase at a constant Q_{H_2O} of 45 μL/min. The concentration distribution of CAMs (a) and the concentration profile of CAMs (b) as a function of the transverse coordinate of the microchannel at Q_{THF} values of 10, 15, 20, 25, 30, and 35 μL/min (from top to bottom). The concentration gradient displays as a color gradient from 0 (red) to 1.0 (blue). The concentration profiles of CAMs in panel b were recorded at the transverse coordinate of the microchannel at a 4.5 mm distance away from the junction at various Q_{THF} values.

The effect of Q_{H_2O} on the self-assembly was further studied. At a constant Q_{THF} of 10 μL/min, the increase of Q_{H_2O} from 20 to 80 μL/min resulted in a gradual decrease of vesicle size from 279.4 to 98.1 nm (Figure 3a). The increase of Q_{H_2O} imposed a stronger focusing effect on the center stream and thus a decrease in the width of the central stream. This led to the formation of smaller vesicular assemblies.[28] Simulation results in Figure 3b show the concentration profile of CAMs by varying Q_{H_2O} at a constant Q_{THF} of 10 μL/min. The increase of Q_{H_2O} decreased the width of the THF stream because of the enhanced focusing effect.

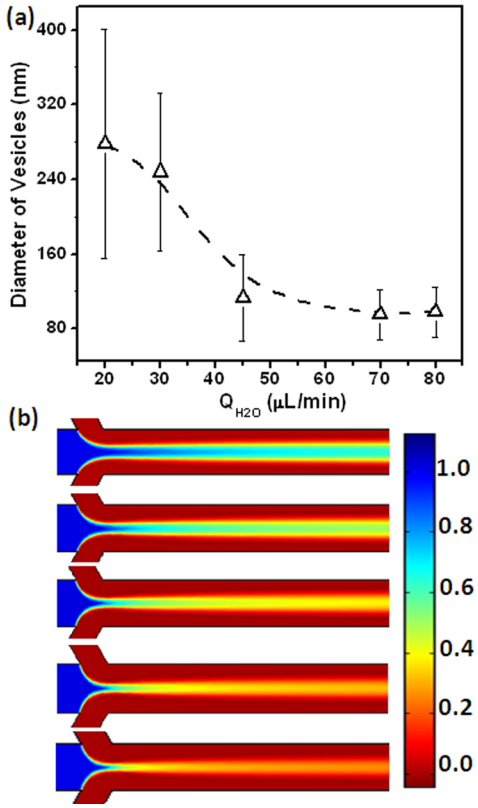

Figure 3. (a) Plotting the size of the vesicles as a function of Q_{H_2O} at a constant Q_{THF} of 10 μL/min. The size of the vesicles at each point was averaged from more than 100 vesicles. (b) Simulated concentration distribution of CAMs in the flow-focusing region at Q_{H_2O} of 20, 30, 45, 60, and 80μL/min (from top to bottom). A Q_{THF} of 10 μL/min was used in all cases.

The competitive diffusion of solvent/CAMs along the transverse direction of the microchannel also plays an important role in the assembly process. The diffusion coefficient (D) of a species (i.e., solvent molecules and CAMs) is inversely proportional to their size (as given in eq

dx.doi.org/10.1021/am4028839 | ACS Appl. Mater. Interfaces 2013, 5, 9746−9751

4); that is, the smaller the diameter of the particles, the larger the diffusion coefficient. For molecular amphiphiles, their size and diffusion rate are generally on the same order of magnitude as the solvent molecules. In this case, there is no clear boundary of the concentration gradient of solvents and amphiphiles. In contrast, the significant increase in the dimension of CAMs drastically decreases their diffusion rate. For instance, the diffusion rate of CAMs with a radius of ~30 nm (including the shell thickness of BCPs) is approximately two orders of magnitude higher than that of low-molecular-weight amphiphiles and organic solvents. The delay in the transverse diffusion of CAMs leads to a significant difference in the gradients of solvents and CAMs. This phenomenon strongly affects the process of kinetically controlled self-assembly. The concentration profile of pure BCPs, CAMs of Au-5 nm, and CAMs of Au-20 nm given in Figure 4a indicates that CAMs

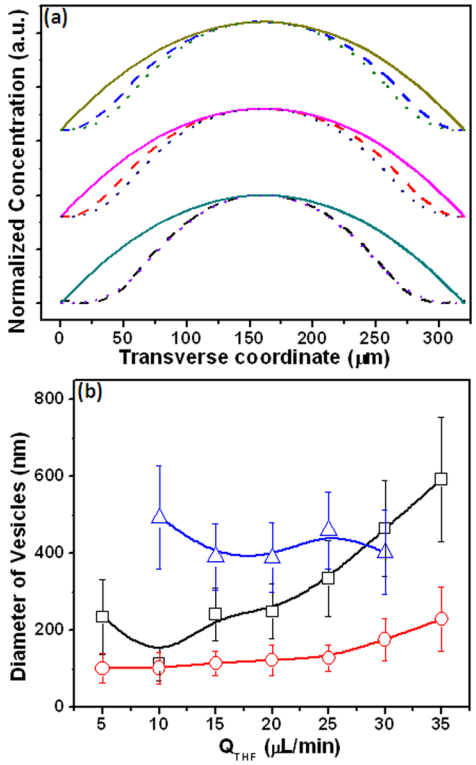

Figure 4. (a) Simulated concentration profiles of pure BCPs (solid line), CAMs of Au-5 nm (dash line), and CAMs of Au-20 nm (dot line) as a function of the transverse coordinate of the microchannel at a 4.5 mm distance away from the junction. From top to bottom, Q_{THF} was 10, 20, and 30 μL/min. A constant Q_{H_2O} of 45 μL/min was used. (b) Plotting the diameter of the assemblies from pure BCPs (○), CAMs of Au-5 nm (□), and CAMs of Au-20 nm (Δ) as a function of Q_{THF} at a constant Q_{H_2O} of 45 μL/min.

with a larger size are more confined within the flow than BCPs. Therefore, we expect that this phenomenon will lead to a slower process for the interacting of the solvents and CAMs with a large diameter and thus the generation of larger assembled structures of CAMs.

Experimentally, we have studied the assembly behavior of amphiphiles with different sizes, including BCPs, CAMs of 5 nm AuNPs, and CAMs of 20 nm AuNPs. Figure 4b shows a comparison of the assembled structures from these building blocks with different dimensions as a function of Q_{THF} at a constant Q_{H_2O} of 45 μL/min. When PEO_{45}-b-PS_{455} was used, the size of BCP vesicles increased from ~103.3 to 228.1 nm with the increase of Q_{THF} from 5 to 35 μL/min. The size of BCP vesicles is much smaller than that of CAMs under the same flow conditions. This can be explained by the difference in the diffusion coefficient of amphiphiles. Amphiphiles with a smaller size can diffuse more rapidly towards water phase because of the larger diffusion rate, leading to the formation of smaller vesicular assemblies. When larger CAMs were used, larger assemblies were generated because of the slower diffusion of CAMs. For example, the size of the structures assembled from CAMs with 20 nm AuNPs increased to the range of ~401.2 to 495.6 nm (Figure 4b). However, the size of the assemblies fluctuated as a function of Q_{THF}, which is not yet fully understood. When even larger CAMs with AuNRs (40 nm in length and 10 nm in diameter) were used as in our previous report,[35] giant vesicles with a diameter in the range of 1 to 2 μm were produced in MFFDs.

CONCLUSIONS

We have systematically studied the continuous assembly of CAMs in MFFDs in experiments and simulations. The hydrodynamic conditions (e.g., flow rates of the fluids and diffusion coefficient of CAMs) that affect the diffusion and mixing of the fluids had great impacts on the self-assembly of CAMs. By varying flow rates of two fluids, the size of CAM vesicles can be controlled in the range of 100−600 nm. In addition, we found that in contrast to molecular amphiphiles, the diffusion coefficient of amphiphilic colloids strongly affects the kinetics of the assembly process. Larger CAMs with a slow diffusion rate generated larger assemblies because of the continuous recruitment of the colloidal building blocks. This work will provide fundamental guidance for the MF assembly of colloidal NPs into functional nanostructures with applications in fields such as bioimaging, drug delivery, and nano- and microreactors.[12,42,43]

ASSOCIATED CONTENT

Supporting Information

SEM and TEM images of different amphiphiles of BCPs, BCP-tethered AuNP-5 nm, and BCP-tethered AuNP-20 nm. This material is available free of charge via the Internet at http://pubs.acs.org.

AUTHOR INFORMATION

Corresponding Author

*E-mail: znie@umd.edu.

Author Contributions

‖These authors contributed equally.

Notes

The authors declare no competing financial interest.

ACKNOWLEDGMENTS

We gratefully acknowledge financial support from the American Chemical Society Petroleum Research Fund (PRF no. 53461-DNI7). We also thank the Maryland NanoCenter and its NispLab for the SEM/TEM imaging. The NispLab is supported in part by the NSF as a MRSEC Shared Experimental Facility.

REFERENCES

(1) Hu, J.; Wu, T.; Zhang, G.; Liu, S. *J. Am. Chem. Soc.* **2012**, *134*, 7624−7627.
(2) Yu, X. F.; Zhong, S.; Li, X. P.; Tu, Y. F.; Yang, S. G.; Van Horn, R. M.; Ni, C. Y.; Pochan, D. J.; Quirk, R. P.; Wesdemiotis, C.; Zhang, W. B.; Cheng, S. Z. D. *J. Am. Chem. Soc.* **2010**, *132*, 16741−16744.
(3) Grzelczak, M.; Sanchez-Iglesias, A.; Mezerji, H. H.; Bals, S.; Perez-Juste, J.; Liz-Marzan, L. M. *Nano Lett.* **2012**, *12*, 4380−4384.
(4) He, J.; Liu, Y.; Babu, T.; Wei, Z.; Nie, Z. *J. Am. Chem. Soc.* **2012**, *134*, 11342−11345.
(5) Song, J. B.; Cheng, L.; Liu, A. P.; Yin, J.; Kuang, M.; Duan, H. W. *J. Am. Chem. Soc.* **2011**, *133*, 10760−10763.
(6) Guo, Y.; Harirchian-Saei, S.; Izumi, C. M. S.; Moffitt, M. G. *ACS Nano* **2011**, *5*, 3309−3318.
(7) Mai, Y.; Eisenberg, A. *J. Am. Chem. Soc.* **2010**, *132*, 10078−10084.
(8) He, J.; Zhang, P.; Babu, T.; Liu, Y.; Gong, J.; Nie, Z. *Chem. Commun.* **2013**, *49*, 576−578.
(9) Liu, K.; Nie, Z. H.; Zhao, N. N.; Li, W.; Rubinstein, M.; Kumacheva, E. *Science* **2010**, *329*, 197−200.
(10) Nie, Z. H.; Fava, D.; Kumacheva, E.; Zou, S.; Walker, G. C.; Rubinstein, M. *Nat. Mater.* **2007**, *6*, 609−614.
(11) Glotzer, S. C.; Solomon, M. J. *Nat. Mater.* **2007**, *6*, 557−562.
(12) Mai, Y.; Eisenberg, A. *Acc. Chem. Res.* **2012**, *45*, 1657−1666.
(13) Li, W.; Zhang, P.; Dai, M.; He, J.; Babu, T.; Xu, Y.-L.; Deng, R.; Liang, R.; Lu, M.-H.; Nie, Z.; Zhu, J. *Macromolecules* **2013**, *46*, 2241−2248.
(14) Zhang, K. K.; Jiang, M.; Chen, D. Y. *Prog. Polym. Sci.* **2012**, *37*, 445−486.
(15) Hu, J. M.; Wu, T.; Zhang, G. Y.; Liu, S. Y. *J. Am. Chem. Soc.* **2012**, *134*, 7624−7627.
(16) Hickey, R. J.; Haynes, A. S.; Kikkawa, J. M.; Park, S. J. *J. Am. Chem. Soc.* **2011**, *133*, 1517−1525.
(17) Grzelczak, M.; Vermant, J.; Furst, E. M.; Liz-Marzán, L. M. *ACS Nano* **2010**, *4*, 3591−3605.
(18) Nie, Z. H.; Petukhova, A.; Kumacheva, E. *Nat. Nanotechnol.* **2010**, *5*, 15−25.
(19) Duxin, N.; Liu, F. T.; Vali, H.; Eisenberg, A. *J. Am. Chem. Soc.* **2005**, *127*, 10063−10069.
(20) Li, W.; Liu, S.; Deng, R.; Zhu, J. *J. Am. Chem. Soc.* **2011**, *50*, 5865−5868.
(21) Chen, G.; Wang, Y.; Yang, M.; Xu, J.; Goh, S. J.; Pan, M.; Chen, H. *J. Am. Chem. Soc.* **2010**, *132*, 3644−3645.
(22) Lee, J.-H.; Chen, K.-J.; Noh, S.-H.; Garcia, M. A.; Wang, H.; Lin, W.-Y.; Jeong, H.; Kong, B. J.; Stout, D. B.; Cheon, J.; Tseng, H.-R. *Angew. Chem., Int. Ed.* **2013**, *52*, 4384−4388.
(23) Song, J. B.; Zhou, J. J.; Duan, H. W. *J. Am. Chem. Soc.* **2012**, *134*, 13458−13469.
(24) Geng, J. L.; Li, K.; Pu, K. Y.; Ding, D.; Liu, B. *Small* **2012**, *8*, 2421−2429.
(25) Hu, S. H.; Gao, X. *J. Am. Chem. Soc.* **2010**, *132*, 7234−7237.
(26) Howse, J. R.; Jones, R. A. L.; Battaglia, G.; Ducker, R. E.; Leggett, G. J.; Ryan, A. J. *Nat. Mater.* **2009**, *8*, 507−511.
(27) Jahn, A.; Stavis, S. M.; Hong, J. S.; Vreeland, W. N.; Devoe, D. L.; Gaitan, M. *ACS Nano* **2010**, *4*, 2077−2087.
(28) Jahn, A.; Vreeland, W. N.; Gaitan, M.; Locascio, L. E. *J. Am. Chem. Soc.* **2004**, *126*, 2674−2675.
(29) Thiele, J.; Steinhauser, D.; Pfohl, T.; Forster, S. *Langmuir* **2010**, *26*, 6860−6863.
(30) Lo, C. T.; Jahn, A.; Locascio, L. E.; Vreeland, W. N. *Langmuir* **2010**, *26*, 8559−8566.
(31) Tang, S. K. Y.; Li, Z.; Abate, A. R.; Agresti, J. J.; Weitz, D. A.; Psaltis, D.; Whitesides, G. M. *Lab Chip* **2009**, *9*, 2767−2771.
(32) Karnik, R.; Gu, F.; Basto, P.; Cannizzaro, C.; Dean, L.; Kyei-Manu, W.; Langer, R.; Farokhzad, O. C. *Nano Lett.* **2008**, *8*, 2906−2912.
(33) Shum, H. C.; Kim, J. W.; Weitz, D. A. *J. Am. Chem. Soc.* **2008**, *130*, 9543−9549.
(34) Wan, J.; Bick, A.; Sullivan, M.; Stone, H. A. *Adv. Mater.* **2008**, *20*, 3314−3318.
(35) He, J.; Wei, Z.; Wang, L.; Tomova, Z.; Babu, T.; Wang, C.; Han, X.; Fourkas, J. T.; Nie, Z. *Angew. Chem., Int. Ed.* **2013**, *52*, 2463−2468.
(36) Xia, Y. N.; Whitesides, G. M. *Angew. Chem., Int. Ed.* **1998**, *37*, 551−575.
(37) Jana, N. R.; Gearheart, L.; Murphy, C. J. *Langmuir* **2001**, *17*, 6782−6786.
(38) Wang, L.; Liu, D. Q.; Wang, X. J.; Han, X. J. *Chem. Eng. Sci.* **2012**, *81*, 157−163.
(39) Takayama, S.; Ostuni, E.; Qian, X. P.; McDonald, J. C.; Jiang, X. Y.; LeDuc, P.; Wu, M. H.; Ingber, D. E.; Whitesides, G. M. *Adv. Mater.* **2001**, *13*, 570−574.
(40) He, J.; Huang, X.; Li, Y. C.; Liu, Y.; Babu, T.; Aronova, M. A.; Wang, S.; Lu, Z.; Chen, X.; Nie, Z. *Angew. Chem., Int. Ed.* **2013**, *135*, 7974−7984.
(41) Squires, T. M.; Quake, S. R. *Rev. Mod. Phys.* **2005**, *77*, 977−1026.
(42) He, J.; Liu, Y.; Hood, T. C.; Zhang, P.; Gong, J.; Nie, Z. *Nanoscale* **2013**, *5*, 5151−5166.
(43) Grzelczak, M.; Liz-Marzan, L. M. *Langmuir* **2013**, *29*, 4652−4663.